

# First-principles study of hydrogen dynamics in monoclinic TiO

S. Vahid Hosseini,<sup>1,2</sup> Andrei Postnikov,<sup>2</sup> and Mohammad Reza Mohammadzadeh<sup>1</sup>

<sup>1</sup>*Superconductivity Research Laboratory (SRL), Department of Physics,  
University of Tehran, North Kargar Ave., P. O. Box 14395-547, Tehran, Iran*  
<sup>2</sup>*LCP-A2MC, Université de Lorraine, 1 Bd Arago, F-57078 Metz Cedex 3, France*

(Dated: January 18, 2023)

The existence of intrinsic vacancies in cubic (monoclinic) TiO suggests opportunity for hydrogen absorption, which was addressed in recent experiments. In the present work, based on first principle calculations, the preferences are studied for the hydrogen absorption sites and diffusion paths between them. The oxygen vacancies are found to be primary hydrogen traps with absorption energy of  $-2.87$  eV. The plausible channels for hydrogen diffusion between adjacent vacancy sites (ordered in the monoclinic TiO structure) are compared with the help of calculations done with the nudge elastic band method. Several competitive channels are identified, with barrier heights varying from  $2.87$  to  $3.71$  eV, that is high enough to ensure relative stability of trapped hydrogen atoms at oxygen vacancy sites. Moreover, the possibility of adsorption of molecular hydrogen was tested and found improbable, in the sense that the  $H_2$  molecules penetrating the TiO crystal are easily dissociated (and released atoms tend to proceed towards oxygen vacancy sites). These results suggest that hydrogen may persist in oxygen vacancy sites up to high enough temperatures.

## I. INTRODUCTION

The present work aims at elucidating hydrogen trapping and mobility in titanium monoxide. This subject falls within a relatively small intersection of vast domains of research. The hydrogen absorption, storage and processing in materials is a tremendous and rapidly evolving field; a recent review by Abe *et al.* [1] may serve a nice introduction into the subject. Transition metal oxides are omnipresent in materials science through their different manifestations, over which a concise review by Goode-nough [2] offers an efficient guideline. In what regards specifically the hydrogen problematics, transition metal oxides typically appear as elements of surface protection of metals or as catalytic agents, e.g., in a promising research field of water splitting on oxide-based electrocatalysis [3], explained, e.g., in recent reviews by Zhu *et al.* [4], Song *et al.* [5] and Shang *et al.* [6]. Burke *et al.* [7] summarized the trends in the activity of different transition metal oxides as catalysts for the *oxygen evolution reaction*. The phenomenon of *hydrogen spillover* came into discussion, in which molecular hydrogen dissociates at the metal surface, and protons diffuse into the catalytic oxide support – see, e.g., Ref. 8 concerning the process on MgO, or Ref. 9 for the reaction on  $VO_2$ . Whittingham [10] described hydrogen motion in metal oxides. Nolan and Browne [11] overviewed chemical reactions relevant in oxides in relation with hydrogen energy problematics.

Still narrowing the subject, the works from this category dealing with titanium are not numerous, and predominantly concern the dioxide. Oelerich *et al.* [12, 13] studied catalytic activity of  $3d$  metal oxides, including  $TiO_2$ , and concluded that a tiny addition of them noticeably enhanced hydrogen sorption kinetics of nanocrystalline magnesium. Yin *et al.* [14] studied, in experiment supported by first-principles calculations, the adsorption of hydrogen on the surface of  $TiO_2$  with possible diffusion into the depth. Feng *et al.* [15] looked into effect

of oxygen vacancies in  $TiO_2$  on the enhancing of electro-catalytic activity for *hydrogen evolution reaction* (HER). Oxygen vacancies also play an important role in shaping the *oxygen evolution reaction* essential for water splitting. A recent review on these issues by Zhu *et al.* [16] covers, among a long list of oxides studied, works on titanium dioxide and oxide-nitride. Hu *et al.* [17] praised micro- and mesoporous Ti oxides as “in many ways ideal candidates for hydrogen storage because they can be made from inexpensive and light metal Ti, and the surface area, pore size, and wall thickness can be systematically controlled”. Li *et al.* [18] studied the hydrogen evolution activity in epitaxially grown  $Ti_2O_3$  polymorphs.

Titanium monoxide enters the picture as Swaminathan *et al.* [19] reported that strongly reduced titania (with nominal composition  $TiO_{1.23}$ , the crystal structure of which reveals X-ray diffraction peaks of disordered TiO) exhibits enhanced HER activity. Recently, Skripov *et al.* [20] investigated hydrogen absorption in substoichiometric TiO ( $TiO_{0.72}H_{0.30}$  and  $TiO_{0.96}H_{0.14}$ ) by a combined use of X-ray and neutron diffraction, neutron vibrational spectroscopy and nuclear magnetic resonance. This work led to the following conclusions: (i) in both nearly stoichiometric and strongly substoichiometric (oxygen-deficient) samples, hydrogen atoms resided exclusively at O vacancy sites; (ii) the hydrogenation of nearly stoichiometric, originally B1 disordered, phase provokes an emergence of an ordered ( $Ti_5O_5$  monoclinic) phase coexisting with the disordered (B1-structure) TiO; (iii) hydrogen diffusion seems to be insignificant; (iv) vibrations of hydrogen atoms occur throughout a broad range of frequencies, presumably as a manifestation of different environments (a possible symmetry-lowering off-center displacement of the trapped hydrogen; a completeness or not of its coordinating Ti octahedron) occurring at different O vacancy sites.

TiO can be crystallized in cubic B1 (NaCl-type) structure, allowing broad limits of deviation from stoichiome-

try in the nominal formula  $\text{TiO}_x$ , namely (citing Watanabe *et al.* [21])  $0.9 \leq x \leq 1.25$  at  $990^\circ\text{C}$  and  $0.7 \leq x \leq 1.25$  at  $1400^\circ\text{C}$ . As mentioned further on in Ref. [21], even in equiatomic compound about 15% of both titanium and oxygen sites are vacant. The vacancies are randomly distributed at high temperatures, however on rapid cooling from 1400 to  $990^\circ\text{C}$ , they get ordered, that results in a monoclinic phase, which is in fact the underlying B1 with 1/6 of sites on each sublattice being vacant. While deficiency on either cation or anion sublattice is not uncommon in materials, the coexistence of vacancies in both sublattices is relatively rare and, among the metal monoxides, is known to occur only in  $\text{TiO}$  [22, 23],  $\text{VO}$  [24] and  $\text{NbO}$  [25].

Theoretical studies of  $\text{TiO}$  have a long history. Neckel *et al.* [26] performed self-consistent electronic structure calculation of  $\text{TiO}$  (among other transition metal oxides and nitrides with B1 structure, assumed perfect and complete). This revealed the essential in the placement and composition of different energy bands. Leung *et al.* [27] compared the relative stability under pressure of several Ti- and O-deficient (stoichiometric) ordered phases, including the “true” monoclinic  $\text{Ti}_5\text{O}_5$  one and several more symmetric ordered-vacancies phases; the energy preference of the monoclinic phase has been demonstrated. Andersson *et al.* [28] offered a more detailed analysis of different vacancy-ordered phases, in comparison with a model of disordered alloy (of vacancies) on each sublattice [29]. Graciani *et al.* [30] in an almost simultaneous work reiterated the established reasons for the structural preference of the monoclinic phase. Kostenko *et al.* [31] concentrated on comparing the ordered monoclinic  $\text{Ti}_5\text{O}_5$  phase against the B1 vacancy-disordered one, whereby the latter was simulated by averaging the results over 20 different supercells of  $(40 \times \text{Ti} + 40 \times \text{O})$  atoms (plus  $8 \times \text{Ti} + 8 \times \text{O}$  vacancy sites). Under this perspective, we considered the monoclinic  $\text{TiO}$  phase to be a perfect model system – not too simplistic yet well defined – for studying hydrogen trapping, vibration, and diffusion. A different choice, that of disordered B1 lattice, would make the results too much dependent on the particular model(s) of disorder used. An ambition of the present work is to challenge the conclusions formulated by Skripov *et al.* [20], on the basis of first-principles calculations, and/or to give these qualitative conclusions a numerical expression. Specifically, we probe adsorption energies of hydrogen at different sites, calculate vibration modes of the crystal doped with hydrogen, identify plausible diffusion paths and estimate corresponding energy barriers.

In its concept, our work has certain similarities with *ab initio* simulation by Kajita *et al.* [32] done for hydrogen adsorption at the  $\text{TiO}_2$  surface, in the sense that different trapping sites have been identified, and the energy barriers between them explored. The difference is in the crystal structure of the underlying oxide and in that we considered 3-dimensional crystal in our simulation, and not a surface represented by a slab.

The present work is organized as follows. Section II explains the crystal structure, adsorption sites and the paths between them. Section III outlines technical details of first-principles calculations. Section IV presents the results of hydrogen binding energy and intersite barriers, with its impact on diffusion. The conclusions are summarized in section V.

## II. CRYSTAL STRUCTURE AND GEOMETRY OF VACANCIES

The stable monoclinic structure of nominally stoichiometric  $\text{TiO}$  (which holds however in the concentration range  $\text{TiO}_{0.7}$  through  $\text{TiO}_{1.25}$ ) has been identified by Watanabe *et al.* [21, 33]. In terms of the lattice parameter of the nominal underlying cubic (B1) lattice, and in the setting to be used in the following, the monoclinic lattice comes about spanned by  $\mathbf{a} = [201]$ ,  $\mathbf{b} = [010]$ , and  $\mathbf{c} = [\bar{1}01]$  vectors. Correspondingly, the unit cell contains  $3 \times 4 = 12$  of both anionic and cationic sites, of which only 10 (of each species) are occupied. Further on,  $a/b = \sqrt{5}$ ,  $c/b = \sqrt{2}$ , and  $\beta = \pi - \arctan(3) = 108^\circ 26'$ . These relations, as we will see, are slightly modified due to the presence of vacancies. The distribution of vacancies centers the  $(a, b)$  face [34], hence the primitive cell in fact includes five Ti and five O atoms. Their arrangement over Wyckoff positions with coordinates refined in experiment can be found in Ref. 21. The unit cell, in several side views (with different diffusion paths, see below) and as a  $[010]$  projection of two consecutive atomic planes  $y=0$  and  $y=\frac{1}{2}$ , is shown in Fig. 1. The choice of the unit cell is such that Ti vacancy is at the origin. These projection figures specify, for further reference, the numbering of  $\text{Ti}_4\text{O}_4$  cuboids (eventually with vacancies, represented by squares instead of circles, at some vertices) centered in the  $y=\frac{1}{4}$  and  $y=\frac{3}{4}$  planes.

A priori, the possible hydrogen absorption sites are expected to possess certain symmetry; plausible candidates are interstitial positions (inside the  $\text{Ti}_4\text{O}_4$  cuboids, probably with one or two corner atoms missing), the Ti vacancy sites, or the O vacancy sites. All these possibilities have been explored (see the details below), with the conclusion that the oxygen vacancies are the ground-state configurations, Ti vacancies are metastable local minima, and the other trial configurations end up squeezed out into one or the other of the two mentioned. Anticipating the question of hydrogen diffusion between the oxygen vacancy sites, we can already elaborate on the possible trajectories connecting such adjacent positions. Fig. 1 summarizes all possible paths connecting adjacent O vacancies, shown as straight-line fragments through the centers of different (numbered) cuboids. In practical calculations using the Nudged Elastic Band (NEB, see below) technique, the trajectories will be shortened / smoothened.

Making reference to numbered cuboids (at the bottom left of Fig. 1) which “pave” two alternating (010) planes

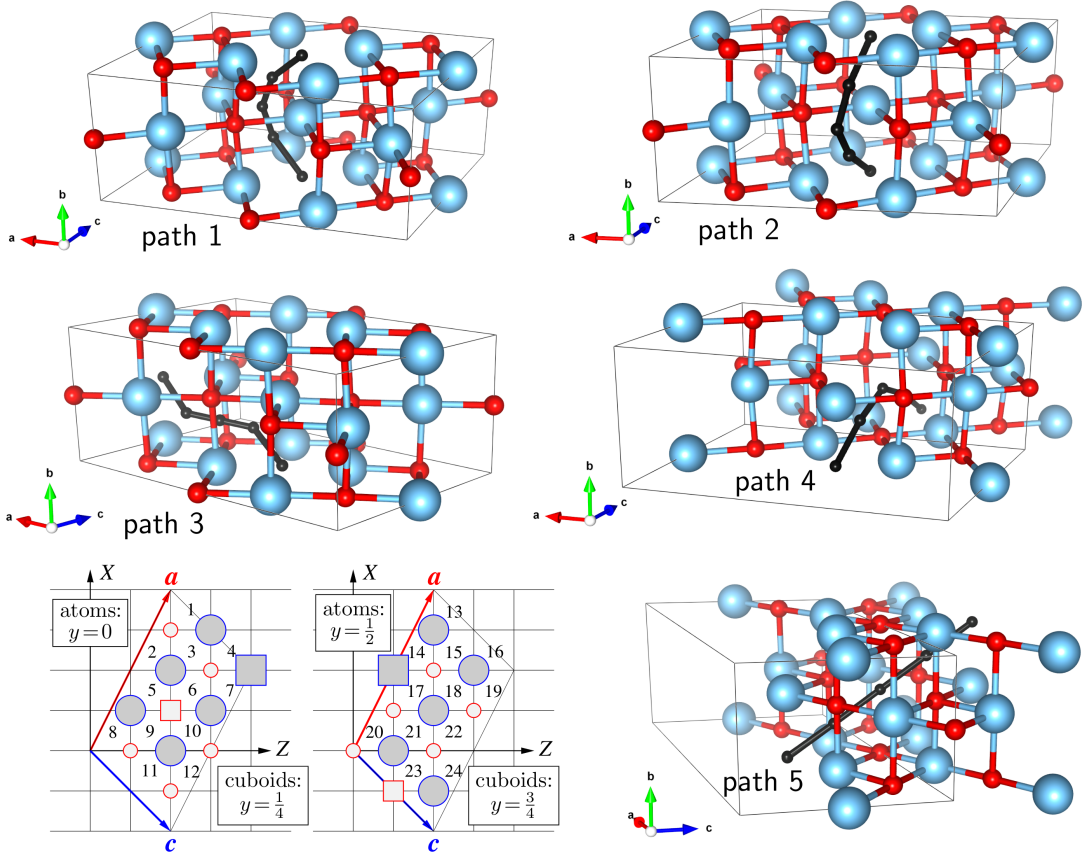


FIG. 1. Crystal structure of monoclinic TiO, in side views (Ti atoms shown large blue and O atoms small red), with five different paths (shown in black color as connected intermediate positions) between adjacent oxygen vacancy sites, and (two panels in the bottom left) as two consecutive (010) planes, with atoms shown as circles and vacancy sites shown as squares. The cuboids (centered  $y = \frac{1}{4}$  and  $y = \frac{3}{4}$ ) between consecutive atomic layers are numbered, for reference in the text.

of the monoclinic structure, the paths under discussion can be identified as follows.

Both path 1 and path 2 connect the O vacancy sites separated by [010] move, circumventing the Ti atom in between. The path 1 goes (“upwards”, from the O vacancy position with  $y=0$ ) through cuboids 6 and 18 (or, equivalently, 9 and 21); the barrier is obviously anticipated on squeezing through the  $\text{Ti}_2\text{O}_2$  face in between. The path 2 goes through cuboids 5 and 17 (or, equivalently, 10 and 22). The saddle point at  $y = \frac{1}{2}$  occurs now on squeezing through a face which is not complete, because the cuboids in question share a titanium vacancy. Consequently, the path is expected to be pushed either towards or away from this vacancy, and the barrier to become lower than for path 1.

A “watershed” between the paths 1 and 2, with their corresponding saddle points, would be on the Ti–O bond, breaking which is likely to cost much energy.

Path 3 is a  $[\frac{1}{2} \frac{1}{2} 0]$  diagonal move, through the cuboids 6 and 3 (or, equivalently, 9 and 11); the bottleneck is squeezing through a complete  $\text{Ti}_2\text{O}_2$  face underway. Consequently, the barrier is expected to be similar to that on path 1.

Path 4 goes in general [001] direction, making a bow around the O atom situated half-way, through the cuboids 10 and 5 (or, equivalently, through the cuboids 22 and 17 under the  $y=0$  plane). This path is likely to go through (or, rather, just close to) the Ti vacancy site (at  $y = \frac{1}{2}$ ) shared by the two cuboids in question. In this sense, the path 4 resembles path 2; the difference is that an oxygen and not titanium atom is circumvented.

Path 5 goes straight straight along [011] through e.g. the cuboids 10 and 17, via the Ti vacancy site situated half-way (in the corner shared by the both cuboids). We note in this relation that passing *exactly* through the Ti vacancy on this path is imposed by symmetry (that was not the case of path 2 and 4), therefore the barrier height must match the difference of hydrogen absorption energies in the Ti and the O vacancies. We’ll come back to this point in discussing the results below.

In practical calculation of hydrogen absorption energies and diffusion, we were careful to use sufficiently large supercells so that the hydrogen atom could be treated as an isolated impurity, and the effects of spurious periodicity within the hydrogen “sublattice” be minimized.

### III. COMPUTATIONAL DETAILS

Electronic total energies and forces (for conjugated-gradient structure relaxation and the extraction of force constants) were calculated within the density functional theory (DFT), using the generalized gradient approximation (GGA) for exchange-correlation functional in the flavor of Perdew–Burke–Ernzerhof (PBE) [35]. Most of the calculations have been technically performed by the help of the Quantum ESPRESSO (QE) package [36, 37], which uses plane waves as basis functions; some additional calculations, in view of support or extension of thus obtained results, have been done with SIESTA code [38, 39], which relies on atom-centered localized basis functions. The ultrasoft pseudopotentials [40] were employed in QE calculations, whereby Ti  $3s$ ,  $3p$ ,  $3d$ ,  $4s$ , O  $2s$ ,  $2p$  and H  $1s$  states were included as valence ones. In SIESTA calculations, norm-conserving pseudopotentials [41] were used, with the attribution of valence states as indicated above, except for the Ti  $3s$  states, which were attributed to the core. The idea of using two methods was brought about by a need of verification, and a possibility to make use of some complementary features. In QE calculations we used  $1 \times 2 \times 2$  supercells (40 TiO formula units), and in SIESTA calculations –  $1 \times 3 \times 2$  ones (60 TiO formula units). The  $\mathbf{k}$ -mesh used for summations over the Brillouin zone according to the Monkhorst–Pack scheme [42] was more dense in the second case ( $6 \times 5 \times 5$  divisions along the reciprocal lattice vectors) than in the first one ( $4 \times 4 \times 4$  mesh points). The planewave cutoff for the basis set construction in QE was set to 60 Ry; the cutoff for kinetic energy and charge density expansion to 720 Ry. The `MeshCutoff` parameter for the expansions of residual charge density in SIESTA was set to 300 Ry. The convergence for energy was chosen as  $10^{-5}$  eV between two ionic steps, and the maximum force allowed on each atoms is 0.01 eV/Å. Comparing with earlier works, we can state that our QE calculation setup is closest to that used by Kostenko *et al.* [31] in what regards the code applied, the exchange-correlation potential and the supercell size. The differences are that there was no extrinsic impurities considered in Ref. 31 optimization done for lattice parameters (of supercells simulating disorder). Therefore we can address the reader to Fig. 7b of Ref. 31 for inspecting the local densities of states (DOS) in the ordered phase, which exhibit a characteristic pseudogap at the Fermi level, discussed in some of the works cited. Partial DOS in the presence of hydrogen impurity, obtained with SIESTA, will be shown and discussed below. Incorporation energy of a hydrogen atom at a vacancy site is expressed as

$$E_{\text{H}}^I = E_{\text{TiO}+\text{H}} - E_{\text{TiO}} - E_{\text{H}}, \quad (1)$$

where  $E_{\text{TiO}+\text{H}}$  is the total energy of TiO supercell containing a H atom,  $E_{\text{TiO}}$  is the total energy of pristine TiO supercell, and  $E_{\text{H}}$  is the energy of isolated H atom. Applying such formula to total energy results obtained with SIESTA (or, with any other method employing atom-

centered basis functions) demands to correct for basis set superposition error (BSSE, see [43]). In practical terms of our case, this involved placing hydrogen basis sets (“ghost atoms” not carrying core charges nor electrons) at two relevant (trial) positions for hydrogen adsorption. Either one (for calculating  $E_{\text{TiO}+\text{H}}$ ) or none (for  $E_{\text{TiO}}$ ) of these positions were in fact occupied by hydrogen atom, the rest being ghosts. Correspondingly,  $E_{\text{H}}$  stems from a calculation for the same supercell of the same shape, in which a single (spin-polarized) genuine hydrogen atom cohabits with 121 ghosts.

The inspection of minimum energy paths (MEP) connecting distinct local minima (typically over a saddle point) can be, from the side of theory, conveniently done by the Nudged Elastic Band (NEB) method, implemented in the QE code. Ref. [44] offers an overview of NEB and other related schemes, which deal with a sequence of intermediate “images”, e.g., conformations of the system subject to interplay of forces “along” and “away from” the path, ensuring the smoothness and the shortness of the latter. In the present calculations, we considered 13 images and (independently) 25 images, in order to check the stability of results against this parameter; `k_min` and `k_max` switches for elastic bands were chosen at 0.2 and 0.3 Ha, respectively.

### IV. RESULTS AND DISCUSSION

Our calculations included unconstrained structure relaxation of (for reference purposes) pristine monoclinic TiO and, in appropriately enlarged supercell, of hydrogen impurity tentatively placed in various lattice positions. It turned out that the hydrogen remains (the most) stable at oxygen vacancy site, but also at a local energy minimum at titanium vacancy site. Hydrogen escapes from other symmetric positions, e.g., in the centrum of a  $\text{Ti}_2\text{O}_2$  face, or cutting a Ti–O bond.

#### A. Adsorption energies, lattice relaxation, electronic structure

Hydrogen incorporation energies calculated according to Eq. (1) yield, with total energies from QE calculations,  $-2.87$  eV at the O vacancy site (hence energetically favorable insertion) and  $+0.75$  eV at the Ti vacancy site (hence costing energy). Even if straightforwardly identifiable from the point of view of calculation, these values might be not so easy to relate to experiment, because of ambiguity and difficult reproducibility of reference situations, e.g., molecular hydrogen penetrating the crystal, dissociating, etc. “Straightforward” SIESTA calculations, performed without correcting for BSSE, are in qualitative agreement with QE results, yielding  $-3.13$  eV and  $+0.20$  eV for adsorption at the O vacancy and the Ti vacancy sites, respectively. SIESTA calculations staged to minimize the systematic error, e.g., done with the equal

TABLE I. Sizes of empty or H-occupied octahedral cages, according to GGA calculations. For comparison, lattice parameters mapped onto a single monoclinic cell are given. See text for details.

System	dimensions (Ti–Ti in Å) of $\square_{\text{O}}$ along...			dimensions (O–O in Å) of $\square_{\text{Ti}}$ along...			reduced lattice parameters (Å)*		
	[10 $\bar{1}$ ]	[102]	[010]	[10 $\bar{1}$ ]	[102]	[010]	<i>a</i>	<i>b</i>	<i>c</i>
Quantum ESPRESSO calculations (1×2×2 supercells)									
pristine	3.905	4.102	4.163	4.247	4.328	4.163	9.319	4.163	5.845
H@ $\square_{\text{O}}$	<u>3.945</u>	4.098	<u>4.110</u>	4.241	4.316	4.162	9.330	4.162	5.839
H@ $\square_{\text{Ti}}$	3.889	4.091	4.171	<u>4.337</u>	<u>4.404</u>	<u>4.309</u>	9.329	4.165	5.853
SIESTA calculations (1×3×2 supercells)									
pristine	3.926	4.239	4.226	4.340	4.489	4.247	9.507	4.224	5.954
H@ $\square_{\text{O}}$	<u>3.997</u>	4.242	<u>4.185</u>	4.321	4.479	4.252	9.510	4.229	5.958
H@ $\square_{\text{Ti}}$	3.921	4.241	4.230	<u>4.398</u>	<u>4.535</u>	<u>4.362</u>	9.511	4.224	5.953
X-ray diffraction by Watanabe <i>et al.</i> <sup>†</sup>									
pristine	4.026	4.197	4.142	4.233	4.256	4.142	9.340	4.142	5.855

\*Crystallographic angle was within +0.06% in QE calculations and within −0.5% in SIESTA calculations from the experimental value  $\beta = 107^\circ 32'$  as reported in <sup>†</sup>Ref. 21; the original attribution of crystallographic parameters is changed in the table to match that in later works.

number and positions of (either real or ghost) atoms in the three situations relevant for Eq. (1), result in adsorption energies of  $-2.86$  eV (H@ $\square_{\text{O}}$ ) and  $+0.73$  eV (H@ $\square_{\text{Ti}}$ ). Such remarkable agreement between the results of technically as different calculations as QE and SIESTA, performed with different pseudopotentials and for supercells of different size, gives certain credibility to these numbers.

In the course of relaxation around the impurity in one or the other position, the crystal environment is not significantly distorted. Still, there are trends reliable beyond the calculation “noise”, which are summarized in Table I. They concern the dimensions of octahedral cages, measured between two opposite atoms flanking either the vacancy, or the hydrogen atom occupying the vacancy site. The distance which noticeably (by  $\simeq 1\%$ ) shrinks as compared to situation in pristine lattice is overlined in the table; those which expanded (by at least the same margin) are underlined. One sees that an insertion of hydrogen either in an oxygen or a titanium vacancy site expands the corresponding surrounding cage primarily along the long diagonal of the monoclinic unit cell. The average lattice parameters (shown in the three last columns of Table I) and the dimensions of the hydrogen-free vacancy cages remain unchanged.

The densities of states (at the hydrogen atom, its nearest neighbors and per each atom species, averaged over the corresponding supercell) are depicted in Fig. 2 and 3. The Ti DOS is characterized by a dip at the position of the Fermi level, marked in earlier calculations [27, 45]. Among the six Ti atoms neighboring the inserted hydrogen, the two closest to it (compacted towards hydrogen along [010], see Table I) develop the most pronounced distinctions (two distinct peaks just above the Fermi level, see Fig. 2f) from the pristine (or, lattice-averaged, cf.

Fig. 2b) Ti DOS.

A marked difference between the two hydrogen placements is that the initial magnetic moment at the hydrogen atom disappears when the latter is inserted at the oxygen vacancy site, but survives at the titanium vacancy site. An inspection of Mulliken populations (comparing the fully relaxed situation of a hydrogen insertion with the pristine crystal and ghost atom at the vacancy site) shows a flow of about 0.09 electrons onto H at the O vacancy site from its surrounding Ti atoms. This seems sufficient to destroy the magnetic moment at the H site. For the H at the Ti vacancy site, on the contrary, no appreciable charge transfer from / to the O nearest neighbors occurs; however, electronic shells of oxygen atoms are spin polarized to (together over the six atoms)  $0.12 \mu_{\text{B}}$ . This polarization is two times stronger on the “out-of-plane” atoms (situated at  $\pm \frac{1}{2} \mathbf{b}$ , marked (f) in Fig. 3 than on the “in-plane” atoms, marked (d) and (e), as can be seen in the corresponding PDOS (note the hybridization with the strong majority-spin peak in the PDOS of hydrogen just below the Fermi level).

## B. Phonons

For additional insight, and also in order to offer some discussion of interesting neutron energy loss spectra published by Skripov *et al.* [20], we calculated density of vibration modes for H-doped (one atom per supercell) monoclinic TiO. The QE calculation used density functional perturbation method, and SIESTA – frozen phonon calculation. In both these cases, just  $\Gamma$  phonons for the corresponding supercell have been calculated, yielding 243 and 363 modes, respectively. The resulting densities of modes are depicted in Fig. 4, slightly broadened

(with halfwidth parameter of  $5 \text{ cm}^{-1}$ ) for better visibility. The abovementioned neutron scattering spectrum is reproduced for comparison, with energy axes properly aligned.

One notes an encouraging agreement between the Ti/O parts of the vibration spectra obtained by two methods, the degree of such agreement being not a priori obvious in view of certain difference in calculating the electronic structure and assessing the phonons. As was correctly anticipated in Ref. [20], the low-energy ( $\approx 60 \text{ meV}$ ) peak in their neutron scattering spectra (cf. Fig 4 and 5 of the work cited) is due to optical vibrations of oxygen atoms. Moreover, based on inspection of vibration patterns in different modes one can now conclude that the split-off peak at the top of the oxygen vibration band at  $\approx 600 \text{ cm}^{-1}$ , which is also pronounced in the experimental spectrum, reveals the vibrations of 4-coordinated

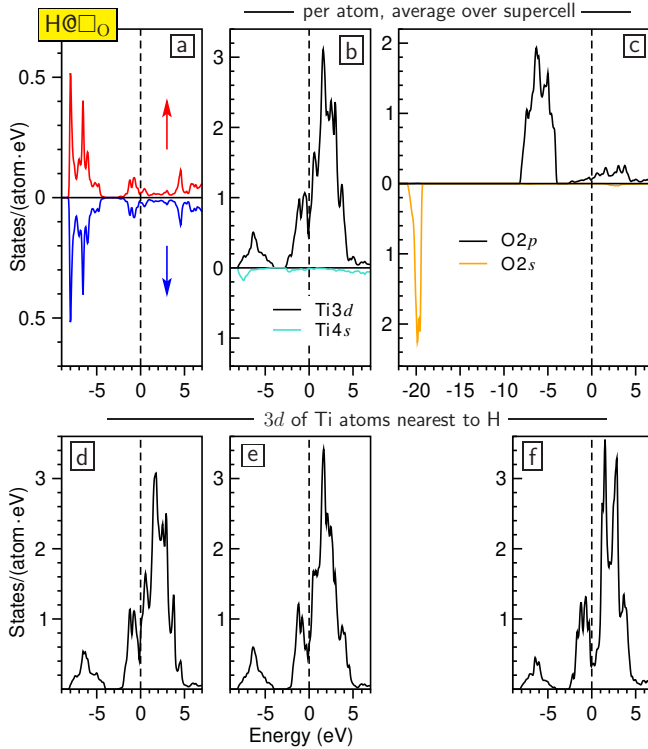


FIG. 2. Partial densities of states (DOS) in relaxed  $1 \times 3 \times 2$  (120 atoms) supercell of monoclinic TiO, containing also a hydrogen atom at the oxygen vacancy site, from a SIESTA calculation. Zero energy (dashed vertical line) corresponds to the Fermi energy. The upper row includes (a) spin-resolved DOS of H atom (in fact non-magnetic in this position); (b) 3d and 4s DOS of Ti (averaged over all Ti sites in the supercell); (c) 2s and 2p DOS of O (averaged over all O sites in the supercell). The bottom row depicts the 3d DOS for three symmetrically distinct pairs of Ti atoms octahedrally bordering the vacancy site occupied by hydrogen, namely (d) atoms situated at  $\pm \frac{1}{6}(\mathbf{a}-\mathbf{c})$ , (e) – at  $\pm \frac{1}{6}(\mathbf{a}+2\mathbf{c})$ , (f) – at  $\pm \frac{1}{2}\mathbf{b}$ , in units of nominal translation vectors of the monoclinic structure (cf. Fig. 1).

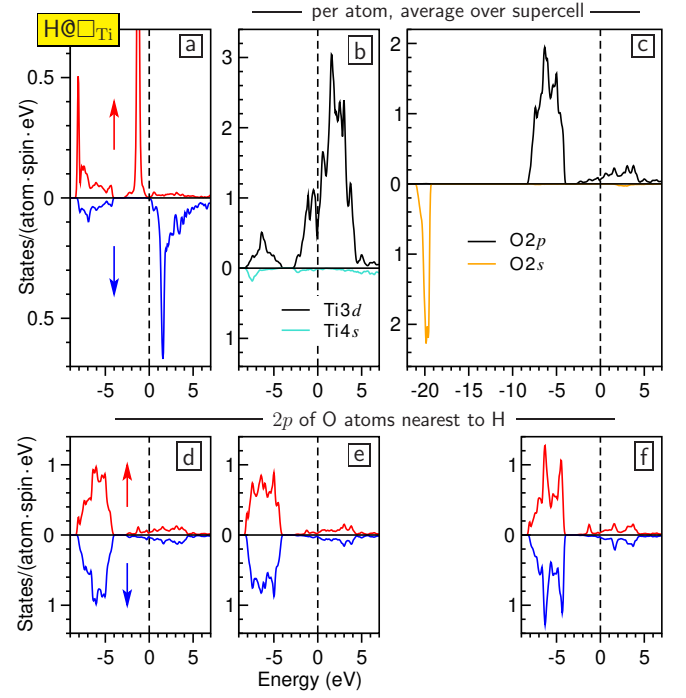


FIG. 3. Similar to Fig. 2, for the case of a hydrogen atom at the titanium vacancy site. The system possesses the magnetic moment of  $1 \mu_B$ . The bottom row depicts 2p DOS of O atoms around the Ti vacancy site, namely (d) atoms situated at  $\pm \frac{1}{6}(\mathbf{a}-\mathbf{c})$ , (e) – at  $\pm \frac{1}{6}(\mathbf{a}+2\mathbf{c})$ , (f) – at  $\pm \frac{1}{2}\mathbf{b}$ .

oxygen atoms, i.e., those bordering to Ti vacancies at  $\pm \frac{1}{2}\mathbf{b}$ .

The interpretation of H-related part of vibration spectra is less straightforward. At least so much is certain that hydrogen vibrations are spatially localized and well separated – by at least  $200 \text{ cm}^{-3}$  – from the continuum of O-related modes. Due to smallness of the hydrogen mass, tiny variations in the concerned force constants transpose into large fluctuations of frequency. In particular, a possible ambiguity in fixing the equilibrium position for phonon calculation, along with technical difference in treating interactions of hydrogen atom with its environment within a planewave-basis method like QE and a fixed-basis method like SIESTA might be responsible for the differences evidenced by the two methods in Fig. 4. Along with an analysis of experimental spectra, these differences however might turn out instructive. The QE makes use of the available crystal symmetry and, in the course of phonon calculation, proceeds from the hydrogen atom placed at the middle of the oxygen vacancy cage. Correspondingly, the hydrogen vibration is a single triply degenerate line. The SIESTA calculation, on the contrary, does not impose any symmetry and proceeds from (technically) slightly off-centered position. The force constants are technically evaluated from finite displacements of atoms, applied in Cartesian directions not related to the crystal cell orientation [46]. Taken together, this yields a considerable splitting of the three



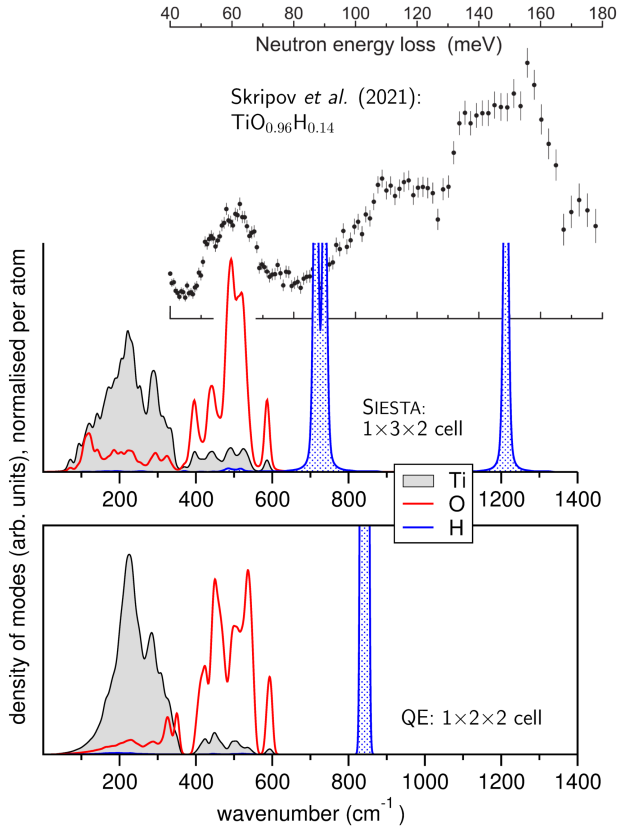


FIG. 4. Densities of vibration modes of TiO with H occupying an oxygen vacancy site (one per supercell indicated), calculated by QE (bottom panel) and SIESTA (middle panel). Neutron scattering spectrum of monoclinic  $\text{TiO}_{0.96}\text{H}_{0.14}$  from Fig. 5 of Ref. [20] is shown for comparison in the upper panel. See text for detail.

H-related modes, revealing different “polarizations” of corresponding vibrations. Remarkably, such “random” (“noisy”) vibration frequencies fall quite well onto the experimental neutron scattering spectrum, which reveals an extremely broad distribution, culminating at frequencies just around the (fortuitously) SIESTA-predicted line at  $1200\text{ cm}^{-1}$ .

It was emphasized in Ref. [20] that “... the volume of the voids formed by oxygen vacancies is too large for H atoms, so that a hydrogen atom can be easily displaced from the geometrical center of the vacancy”. The diversity of such displacements was considered as a possible reason for the broadness of the H-related vibration spectra. This explanation seems plausible.

A neutron energy loss spectrum (cf. Fig. 4 of Ref. [20]) of strongly substoichiometric and strongly hydrogen-saturated  $\text{TiO}_{0.72}\text{H}_{0.30}$ , which is not pronouncedly monoclinic but B1-cubic with disordered vacancies, retaining the general width, becomes more “compacted” and centered around  $120\text{ meV}$ . This brings the shape of the spectrum closer to a more “symmetric” one suggested by a QE calculation.

### C. Dissociation of $\text{H}_2$ molecule

In the study of hydrogen uptake and diffusion in metals, it is generally accepted that the  $\text{H}_2$  molecule is first physisorbed at the surface and may then overcome the activation barrier for dissociation (see, e.g., a discussion around Fig. 1 of Kirchheim and Pundt [47]). Hydrogen atoms may further on be chemisorbed and eventually diffuse into the material. As in the discussion about hydrogen diffusion (see next subsection), quantum effects may be important in overcoming the activation barrier; an early representative work to this effect, simulating dissociative adsorption (of  $\text{H}_2$  on Cu surface), was done by Mills and Jónsson [48]. We do not address this issue here in details, but, as the geometry and the properties of TiO are somehow different from common metals, we wonder whether a hydrogen molecule may fit into, and survive intact within, the oxygen vacancy cage.

As it turns out in the course of conjugate-gradient total energy minimization (see Fig. 5, one example out of several trial ones starting from different initial orientations), the molecule eventually “almost dissociates”, doubling the nominal H–H bond length to  $\simeq 1.4\text{ \AA}$ . It looks like every hydrogen atom preferentially “couples” to three closest Ti atoms, in the spirit of the remark made in the previous subsection about the oxygen vacancy cage being too large for a hydrogen atom. We did not manage to reproduce a definite dissociation, when one of the H atoms would flee the  $\text{Ti}_6$  cage delimiting an oxygen vacancy site, because this would require an energy inflow to overcome a barrier (see next subsection); however, such event seems to be within grasp for a molecular dynamical high-temperature simulation. Indeed, an energy step of  $\simeq 1.2\text{ eV}$  (see Fig. 5) separates the “weakened”/expanded

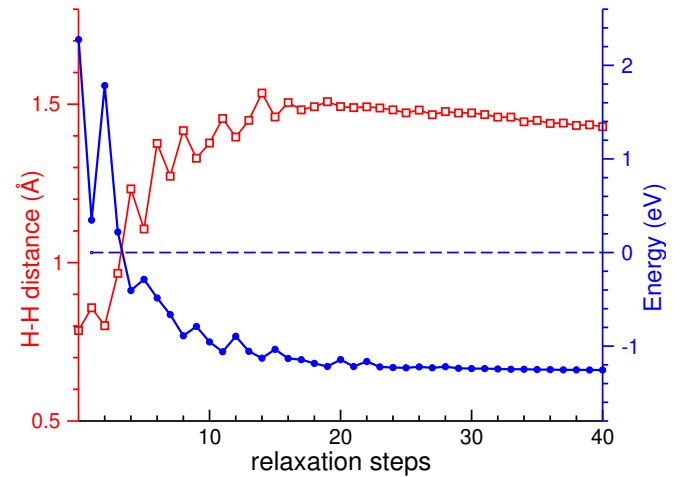


FIG. 5. Evolution of interatomic distance (left scale, red squares) and total energy (right scale, blue dots) of an  $\text{H}_2$  molecule placed in an oxygen vacancy, after a SIESTA calculation. Zero energy corresponds to a situation with a single H atom relaxed at oxygen vacancy site and another one being free. See text for details.

H<sub>2</sub> molecule from a situation when one of its constituent H atoms is promoted out of the crystal. An irrevocable dissociation and diffusion away from the original site of an atom remaining within the crystal may presumably cost less energy.

#### D. Energy barriers for hydrogen atom hopping over oxygen vacancy sites

We turn now to the discussion of scenarios, outlined earlier in Section II, of how a hydrogen atom, initially trapped in oxygen vacancy site, can be brought onto an adjacent similar site. Practical calculations have been done according to NEB formalism implemented in QE code; comparison of results obtained with 13 and with 25 images along the path gives us credibility in what regards the barrier height, whereby the barrier profile obtained with 25 images is more smooth and permits to discuss some details. All the paths must in principle be left-right symmetric; this is not exactly the case for paths 4 and 5, due to numerical “noise” in the course of practical NEB calculations. From the end points, the energy profile departs nicely parabolically, which is not so obvious with 13 images but much better represented for 25-images path (cf. bottom right panel in Fig. 6). Assuming that the hydrogen atom vibrates *alone* around its equilibrium position at the extremity of each path, the corresponding frequency from fitting the corresponding force constant falls between 776 cm<sup>-1</sup> (along the path 4 or 5) to 816 cm<sup>-1</sup> (along the path 3). This nicely matches the prediction from the “full” phonon calculation addressed above.

We turn now to a discussion of different paths. The paths 4 and 5 seem degenerate; that follows indeed from an observation that the mid-point in each of them is the same, – namely, a Ti vacancy site, from which the path can equally turn “downwards” or “upwards”, consistently to drawings in the two last panels of Fig. 1. One sees a shallow local minimum on top of the barrier, which reinforces the previously made observation that this is a metastable position for a hydrogen atom, rather than a genuine saddle point. However, there is a subtlety. If the mid-point of path 5 is placed at the Ti vacancy site by the crystal symmetry, the mid-point of path 4 is subject to technical “drift”, depending on the spring constant along the NEB, or other details of the algorithm used. As a result, the path may tend to get shortened by displacing its midpoint slightly “downwards” (closer to the oxygen atom, as is suggested by a drawing of path 4 in Fig. 1), correspondingly climbing the midpoint energy upwards. Such a “perturbation” would eventually destroy the local minimum on top of the barrier. This was not the case in our calculation which preserved the similarity of the energy profiles along path 4 and path 5. We note that the barrier height in corresponding NEB calculations, 3.71 eV, is expectedly close to the difference between previously discussed adsorption energies at the Ti vacancy

and the O vacancy sites, i.e.,  $+0.75 - (-2.87) = 3.62$  eV. The mismatch of 0.09 eV may be attributed to the technical difference between the constraints imposed in the course of “conventional” conjugate-gradient search and in a NEB calculation.

The “bottleneck” of the paths 1 and 3 is the hydrogen atom squeezing through the intact Ti–O–Ti–O square face. The difference is that on the “upward” (see Fig. 1) path 1 this face is within a (010) lattice plane, whereas for path 3 it makes a (20 $\bar{1}$ ) plane. In path 2, the hydrogen atom passes through an incomplete square face, missing a Ti atom at one of its corners. The snapshots of the atomic relaxation within the corresponding planes is shown in Fig. 7, in comparison with the unperturbed (no hydrogen) situation. One notes that, on passing through the “bottleneck”, the hydrogen atom only slightly repels its Ti neighbors (Ti–Ti diagonal increases by  $\sim 3\%$ ) but quite considerably ( $\sim 27\%$  of the initial distance) pushes apart the O neighbors. This repulsion can be understood from purely electrostatic arguments, since hydrogen, like oxygen, is more electronegative than titanium and receives some electron density from the latter. For this reason, skirting an oxygen atom in the mid-point of path 4 does not bring this path considerably to the side (downwards in Fig. 1), as discussed above, whereas the path 2, laid in fact across a cavity with missing Ti atom, comes quite close to the remaining Ti atom, which the path skirts.

With the “bottlenecks” on path 1 and path 3 being so similar (cf. Fig. 7), we cannot suggest any obvious reason for the difference in corresponding barrier heights other than the “natural” anisotropy of the crystal structure. In any case, the path 2 undoubtedly possesses the lowest energy barrier, since it does not include a passage between closely placed two Ti and two O atoms, pushing those latter to the sides. Consequently, the path 2 is expected to dominate among hypothetical channels of hydrogen diffusion, to which the other paths, possessing the barrier energy of the same order of magnitude, should contribute in parallel without being a priori excluded.

The height of the barrier measured from the endpoint minima, i.e. the activation energy  $E_a$ , may in principle serve to estimate the reaction (e.g., diffusion) rate  $D$  via the Arrhenius equation (see, e.g., the review by Gomer [49] for detail):

$$D = \nu \exp\left(-\frac{E_a}{k_B T}\right). \quad (2)$$

A more detailed analysis of different contributions to the flux of hydrogen atoms induced by gradient of concentrations and involving hoppings over the barriers was given by Kirchheim and Pundt [47], culminating in Eq. (55) of their work. The frequency prefactor  $\nu$  (called “attempt frequency” in Ref. [47]) may vary in very broad ranges, depending on the reaction type; estimations for proton diffusion in TiO might be not obvious. Zhdanov [50] summarized a number of parameters from the literature in Tables 1 and 2 of his review work; for instance, for des-



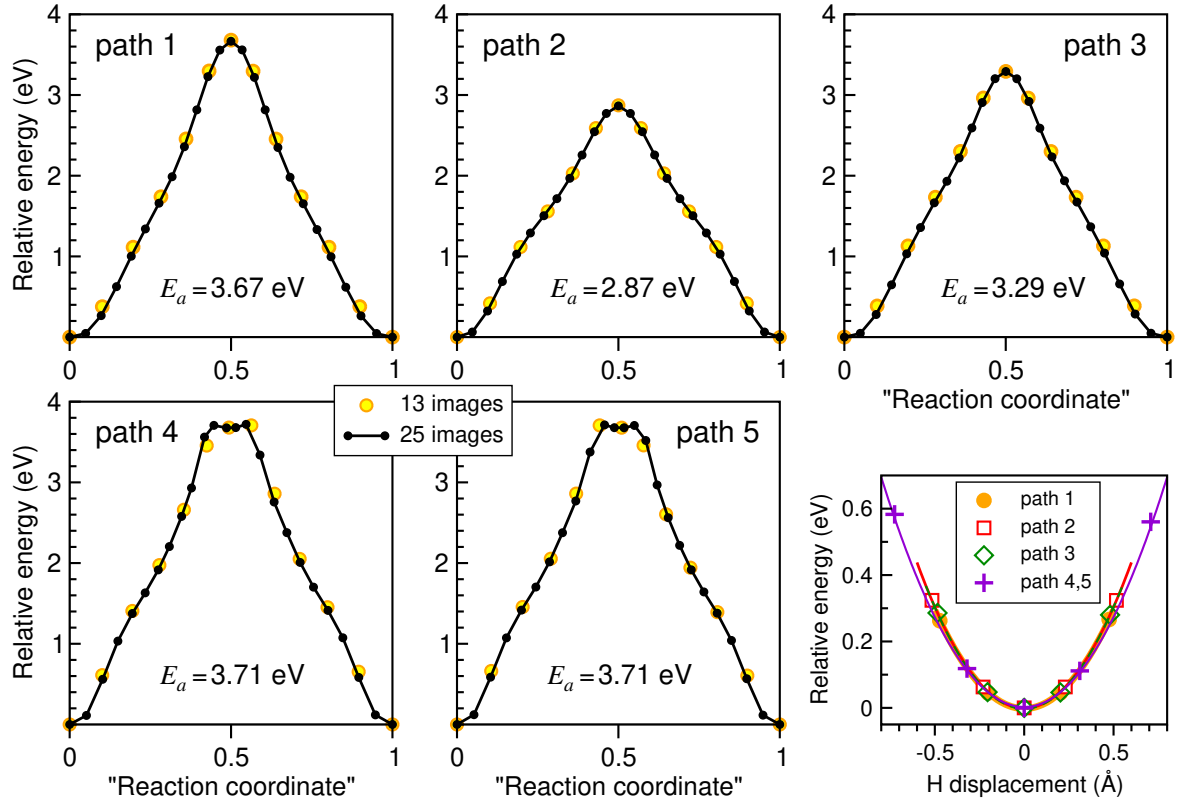


FIG. 6. NEB energy profiles for H atom displacement along the five paths specified in Fig. 1. Results of calculations performed with 13 and with 25 images along each path are shown for comparison. The barrier height is indicated for each path. In the bottom right panel, the total energy is traced as function of absolute displacement of the hydrogen atom from equilibrium position, near the beginning and the end of each path.

orption of  $H_2$  from Pt  $\nu$  makes  $10^6 \text{ s}^{-1}$  and from other different metal surfaces –  $10^{12}$  to  $10^{17} \text{ s}^{-1}$ . In any case, huge heights of the barriers relative to the ambient thermal energy ( $k_B T = 26 \text{ meV}$  at  $25^\circ\text{C}$ ) in practical sense identifies the diffusion over barriers as an utterly improbable event. A general understanding is that quantum

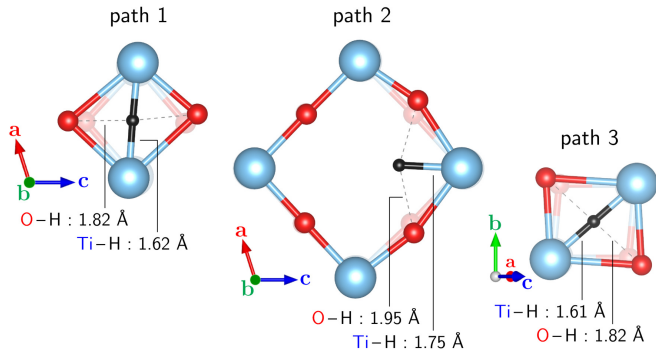


FIG. 7. Optimized structures at the saddle points of paths 1, 2, and 3. Distances between the hydrogen atom and its nearest Ti and O neighbors are indicated. The corresponding equilibrium structures in the absence of hydrogen are shown faded in the background.

tunneling plays an important role in hydrogen transport in metals [51, 52]. A more detailed analysis along this line would go beyond the scope of the present work, but it is likely to be responsible for much higher mobility of hydrogen in different materials than it could be understood in terms of hopping over the barriers. Coming back specifically to TiO, Skripov *et al.* [20] set  $\sim 10^5 \text{ s}^{-1}$  as the upper limit on the hydrogen jump rate in strongly substoichiometric and nearly stoichiometric H-doped TiO, referring to the NMR line width: “...H atoms in titanium monoxides appear to be immobile on the NMR frequency scale up to 370 K”. As an explanation, Skripov *et al.* evoke spatial separation between the oxygen vacancy sites. We reinforce this conclusion by identifying barrier heights as unusually high, by the standards of hydrogen diffusion in metals. For comparison, Pozzo *et al.* [53] calculated the diffusion barriers for hydrogen atoms over the Mg(0001) surface doped with different transition metals to span the values from nearly zero (Ag doping) to – the largest among the systems probed – 0.94 eV (Zr doping) and 0.75 eV (Ti doping).

In view of high barriers separating the hydrogen adsorption sites, and in agreement with the experimental evidence so far available, TiO seems to be promising for accumulating hydrogen, even if not so in terms of easiness

of the hydrogen diffusion. This can give rise to interesting applications, with a perspective of extension over other related materials. Interestingly, the group of Lefort *et al.* reported [54, 55] an enormous capacity to accommodate hydrogen (up to 2.9 wt.%) for highly substoichiometric titanium carbide,  $\text{TiC}_{0.6}$ , which was not the case in weakly substoichiometric  $\text{TiC}_{0.9}$ . The authors attribute this property to the presence of long-range-ordered carbon vacancies in  $\text{TiC}_{0.6}$ , in contrast to  $\text{TiC}_{0.9}$ . In view of the similarity of the crystal structures of titanium carbide and monoxide, this discovery is stimulating for the extension of our present study.

## V. CONCLUSIONS

Summarizing, we performed first-principles calculations of electronic structure, lattice vibrations and possible diffusion barriers in monoclinic TiO doped with H atom. Our results reinforce the earlier available experimental evidence that hydrogen atoms enter the oxygen vacancy sites, the related energy gain now being estimated as  $\simeq 2.87$  eV. Moreover, the Ti vacancy sites were identified as possible metastable positions for adsorbed hydrogen atoms, unfavorable in energy (with respect to the case of desorbed hydrogen) by 0.75 eV. The Ti vacancy site makes a mid-point of two possible diffusion paths (those with the highest barrier, 3.71 eV) connecting two adjacent O vacancy sites. The lowest-energy path (with the barrier height of 2.87 eV) goes around a Ti atom at a distance of 1.75 Å from it. Different paths involve squeezing the H atom through different crystal structure bottlenecks, whereby the O atoms are considerably pushed away and the Ti atoms are somehow attracted towards the hydrogen atom. The estimated values of barrier height are too high to account for an ap-

preciable hydrogen diffusion rate, assuming the hoppings over barriers as the principal diffusion mechanism. It seems plausible that quantum tunneling processes may play an important role, as is the case with hydrogen diffusion in other materials. Calculations of lattice vibration spectrum are consistent with earlier reported results of inelastic neutron diffraction; the remaining deviations offer a substance for discussion about the placement of hydrogen atoms within the oxygen-vacancy cages.

Under an angle of possible applications, our study demonstrates that (and explains why) the Ti monoxide may absorb considerable amount of hydrogen, which however tends to remain immobile in the sense of diffusivity through the lattice. This might be promising, e.g., for superconductivity, the tendency for which can be addressed in a separate study. As another prospective extension towards practical needs, the uptake and dissociation of molecular hydrogen at the surface, an issue almost routinely simulated with some other materials, may seem interesting here. In the context of fundamental science, the manifestation of quantum effects in the uptake and diffusion of hydrogen may deserve a thorough study; moreover, an interplay of vacancy ordering and diffusion may happen to be interesting. In any case, an enrichment of experimental evidence will be highly motivating.

## ACKNOWLEDGMENTS

The authors thank Dr. Alexander Skripov for careful reading of the manuscript and for useful comments. S.V.H. and M.R.M. acknowledge a partial financial support by the Research Council of the University of Tehran. S.V.H. and A.P. thank the mesocenter of calculation EXPLOR at the Université de Lorraine (project 2019CP-MXX0918) for granting access to computational resources.

- 
- [1] J. O. Abe, A. P. I. Popoola, E. Ajenifuja, and O. M. Popoola, Hydrogen energy, economy and storage: Review and recommendation, *International Journal of Hydrogen Energy* **44**, 15072 (2019).
  - [2] J. B. Goodenough, Perspective on engineering transition-metal oxides, *Chemistry of Materials* **26**, 820 (2014).
  - [3] Y. Sun, T. Zhang, C. Li, K. Xu, and Y. Li, Compositional engineering of sulfides, phosphides, carbides, nitrides, oxides, and hydroxides for water splitting, *J. Mater. Chem. A* **8**, 13415 (2020).
  - [4] Y. Zhu, Q. Lin, Y. Zhong, H. A. Tahini, Z. Shao, and H. Wang, Metal oxide-based materials as an emerging family of hydrogen evolution electrocatalysts, *Energy Environ. Sci.* **13**, 3361 (2020).
  - [5] J. Song, C. Wei, Z.-F. Huang, C. Liu, L. Zeng, X. Wang, and Z. J. Xu, A review on fundamentals for designing oxygen evolution electrocatalysts, *Chem. Soc. Rev.* **49**, 2196 (2020).
  - [6] X. Shang, J.-H. Tang, B. Dong, and Y. Sun, Recent advances of nonprecious and bifunctional electrocatalysts for overall water splitting, *Sustainable Energy & Fuels* **4**, 3211 (2020).
  - [7] M. S. Burke, L. J. Enman, A. S. Batchellor, S. Zou, and S. W. Boettcher, Oxygen evolution reaction electrocatalysis on transition metal oxides and (oxy)hydroxides: Activity trends and design principles, *Chemistry of Materials* **27**, 7549 (2015), <https://doi.org/10.1021/acs.chemmater.5b03148>.
  - [8] S. Wu, K.-Y. Tseng, R. Kato, T.-S. Wu, A. Large, Y.-K. Peng, W. Xiang, H. Fang, J. Mo, I. Wilkinson, Y.-L. Soo, G. Held, K. Suenaga, T. Li, H.-Y. T. Chen, and S. C. E. Tsang, Rapid interchangeable hydrogen, hydride, and proton species at the interface of transition metal atom on oxide surface, *Journal of the American Chemical Society* **143**, 9105 (2021), pMID: 34047552, <https://doi.org/10.1021/jacs.1c02859>.
  - [9] H. Yoon, Y. Kim, E. J. Crumlin, D. Lee, K. Ihm, and J. Son, Direct probing of oxygen loss from the surface

- lattice of correlated oxides during hydrogen spillover, *The Journal of Physical Chemistry Letters* **10**, 7285 (2019).
- [10] M. S. Whittingham, Hydrogen motion in oxides: from insulators to bronzes, *Solid State Ionics* **168**, 255 (2004), proceedings of the Workshop on Hydrogen: Ionic, Atomic and Molecular Motion.
  - [11] H. Nolan and M. P. Browne, Hydrogen energy currency: Beyond state-of-the-art transition metal oxides for oxygen electrocatalysis, *Current Opinion in Electrochemistry* **21**, 55 (2020).
  - [12] W. Oelerich, T. Klassen, and R. Bormann, Metal oxides as catalysts for improved hydrogen sorption in nanocrystalline Mg-based materials, *Journal of Alloys and Compounds* **315**, 237 (2001).
  - [13] W. Oelerich, T. Klassen, and R. Bormann, Hydrogen sorption of nanocrystalline Mg at reduced temperatures by metal-oxide catalysts, *Advanced Engineering Materials* **3**, 487 (2001).
  - [14] X.-L. Yin, M. Calatayud, H. Qiu, Y. Wang, A. Birkner, C. Minot, and C. Wöll, Diffusion versus desorption: Complex behavior of H atoms on an oxide surface, *ChemPhysChem* **9**, 253 (2008).
  - [15] H. Feng, Z. Xu, L. Ren, C. Liu, J. Zhuang, Z. Hu, X. Xu, J. Chen, J. Wang, W. Hao, Y. Du, and S. X. Dou, Activating titania for efficient electrocatalysis by vacancy engineering, *ACS Catalysis* **8**, 4288 (2018).
  - [16] K. Zhu, F. Shi, X. Zhu, and W. Yang, The roles of oxygen vacancies in electrocatalytic oxygen evolution reaction, *Nano Energy* **73**, 104761 (2020).
  - [17] X. Hu, M. Trudeau, and D. M. Antonelli, Hydrogen storage in microporous titanium oxides reduced by early transition metal organometallic sandwich compounds, *Chemistry of Materials* **19**, 1388 (2007).
  - [18] Y. Li, Z. G. Yu, L. Wang, Y. Weng, C. S. Tang, X. Yin, K. Han, H. Wu, X. Yu, L. M. Wong, D. Wan, X. R. Wang, J. Chai, Y.-W. Zhang, S. Wang, J. Wang, A. T. S. Wee, M. B. H. Breese, S. J. Pennycook, T. Venkatesan, S. Dong, J. M. Xue, and J. Chen, Electronic-reconstruction-enhanced hydrogen evolution catalysis in oxide polymorphs, *Nature Communications* **10**, 3149 (2019).
  - [19] J. Swaminathan, R. Subbiah, and V. Singaram, Defect-rich metallic titania ( $\text{TiO}_{1.23}$ ) – an efficient hydrogen evolution catalyst for electrochemical water splitting, *ACS Catalysis* **6**, 2222 (2016).
  - [20] A. V. Skripov, A. V. Soloninin, A. A. Valeeva, A. I. Gusev, A. A. Rempel, H. Wu, and T. J. Udovic, Hydrogen in nonstoichiometric cubic titanium monoxides: X-ray and neutron diffraction, neutron vibrational spectroscopy and NMR studies, *Journal of Alloys and Compounds* **887**, 161353 (2021).
  - [21] D. Watanabe, J. R. Castles, A. Jostsons, and A. S. Malin, The ordered structure of  $\text{TiO}$ , *Acta Crystallographica* **23**, 307 (1967).
  - [22] S. P. Denker, Relation of bonding and electronic band structure to the creation of lattice vacancies in  $\text{TiO}$ , *Journal of Physics and Chemistry of Solids* **25**, 1397 (1964).
  - [23] A. A. Valeeva, A. A. Rempel, M. A. Müller, K. J. Reichle, G. Tang, W. Sprengel, and H.-E. Schaefer, Identification of atomic vacancies in titanium monoxide by electron microdiffraction and positron annihilation, *physica status solidi (b)* **224**, R1 (2001).
  - [24] M. D. Banus, T. B. Reed, and A. J. Strauss, Electrical and magnetic properties of  $\text{TiO}$  and  $\text{VO}$ , *Phys. Rev. B* **5**, 2775 (1972).
  - [25] A. Gusev, Niobium monoxide superstructures, *JETP Letters* **111**, 176 (2020).
  - [26] A. Neckel, P. Rastl, R. Eibler, P. Weinberger, and K. Schwarz, Results of self-consistent band-structure calculations for  $\text{ScN}$ ,  $\text{ScO}$ ,  $\text{TiC}$ ,  $\text{TiN}$ ,  $\text{TiO}$ ,  $\text{VC}$ ,  $\text{VN}$  and  $\text{VO}$ , *Journal of Physics C: Solid State Physics* **9**, 579 (1975).
  - [27] C. Leung, M. Weinert, P. B. Allen, and R. M. Wentzcovitch, First-principles study of titanium oxides, *Phys. Rev. B* **54**, 7857 (1996).
  - [28] D. A. Andersson, P. A. Korzhavyi, and B. Johansson, Thermodynamics of structural vacancies in titanium monoxide from first-principles calculations, *Phys. Rev. B* **71**, 144101 (2005).
  - [29] One can add in this relation that a much earlier attempt of a “vacancy-alloying” approach to electronic structure of  $\text{TiO}$ , non self-consistent and within virtual crystal approximation, was undertaken by Schoen and Denker[56].
  - [30] J. Graciani, A. Márquez, and J. F. Sanz, Role of vacancies in the structural stability of  $\alpha\text{-TiO}$ : A first-principles study based on density-functional calculations, *Phys. Rev. B* **72**, 054117 (2005).
  - [31] M. G. Kostenko, A. V. Lukoyanov, V. P. Zhukov, and A. A. Rempel, Vacancies in ordered and disordered titanium monoxide: Mechanism of b1 structure stabilization, *Journal of Solid State Chemistry* **204**, 146 (2013).
  - [32] S. Kajita, T. Minato, H. S. Kato, M. Kawai, and T. Nakayama, First-principles calculations of hydrogen diffusion on rutile  $\text{TiO}_2(110)$  surfaces, *The Journal of Chemical Physics* **127**, 104709 (2007).
  - [33] D. Watanabe, J. R. Castles, A. Jostsons, and A. S. Malin, Ordered structure of titanium oxide, *Nature* **210**, 934 (1966).
  - [34] Space group  $C2/m$ , unique axis  $b$ .
  - [35] J. P. Perdew, K. Burke, and M. Ernzerhof, Generalized gradient approximation made simple, *Phys. Rev. Lett.* **77**, 3865 (1996).
  - [36] P. Giannozzi, S. Baroni, N. Bonini, M. Calandra, R. Car, C. Cavazzoni, D. Ceresoli, G. L. Chiarotti, M. Cococcioni, I. Dabo, A. Dal Corso, S. de Gironcoli, S. Fabris, G. Fratesi, R. Gebauer, U. Gerstmann, C. Gougousis, A. Kokalj, M. Lazzeri, L. Martin-Samos, N. Marzari, F. Mauri, R. Mazzarello, S. Paolini, A. Pasquarello, L. Paulatto, C. Sbraccia, S. Scandolo, G. Sclauzero, A. P. Seitsonen, A. Smogunov, P. Umari, and R. M. Wentzcovitch, Quantum ESPRESSO: a modular and open-source software project for quantum simulations of materials, *Journal of Physics: Condensed Matter* **21**, 395502 (2009).
  - [37] P. Giannozzi, O. Andreussi, T. Brumme, O. Bunau, M. Buongiorno Nardelli, M. Calandra, R. Car, C. Cavazzoni, D. Ceresoli, M. Cococcioni, N. Colonna, I. Carnimeo, A. Dal Corso, S. de Gironcoli, P. Delugas, R. A. DiStasio Jr, A. Ferretti, A. Floris, G. Fratesi, G. Fugallo, R. Gebauer, U. Gerstmann, F. Giustino, T. Gorni, J. Jia, M. Kawamura, H.-Y. Ko, A. Kokalj, E. Küçükbenli, M. Lazzeri, M. Marsili, N. Marzari, F. Mauri, N. L. Nguyen, H.-V. Nguyen, A. Otero-de-la Roza, L. Paulatto, S. Poncé, D. Rocca, R. Sabatini, B. Santra, M. Schlipf, A. P. Seitsonen, A. Smogunov, I. Timrov, T. Thonhauser, P. Umari, N. Vast, X. Wu, and S. Baroni, Advanced capabilities for materials modelling with Quantum ESPRESSO, *Journal of Physics: Condensed Matter* **29**, 465901 (2017).
  - [38] J. M. Soler, E. Artacho, J. D. Gale, A. García, J. Jun-

- quera, P. Ordejón, and D. Sánchez-Portal, The SIESTA method for *ab initio* order- $N$  materials simulation, *Journal of Physics: Condensed Matter* **14**, 2745 (2002).
- [39] A. García, N. Papior, A. Akhtar, E. Artacho, V. Blum, E. Bosoni, P. Brandimarte, M. Brandbyge, J. I. Cerdá, F. Corsetti, R. Cuadrado, V. Dikan, J. Ferrer, J. Gale, P. García-Fernández, V. M. García-Suárez, S. Garcí, G. Huhs, S. Illera, R. Korytár, P. Koval, I. Lebedeva, L. Lin, P. López-Tarifa, S. G. Mayo, S. Mohr, P. Ordejón, A. Postnikov, Y. Pouillon, M. Pruneda, R. Robles, D. Sánchez-Portal, J. M. Soler, R. Ullah, V. W.-z. Yu, and J. Junquera, Siesta: Recent developments and applications, *The Journal of Chemical Physics* **152**, 204108 (2020).
- [40] D. Vanderbilt, Soft self-consistent pseudopotentials in a generalized eigenvalue formalism, *Phys. Rev. B* **41**, 7892 (1990).
- [41] N. Troullier and J. L. Martins, Efficient pseudopotentials for plane-wave calculations, *Phys. Rev. B* **43**, 1993 (1991).
- [42] H. J. Monkhorst and J. D. Pack, Special points for Brillouin-zone integrations, *Phys. Rev. B* **13**, 5188 (1976).
- [43] F. B. van Duijneveldt, J. G. C. M. van Duijneveldt-van de Rijdt, and J. H. van Lenthe, State of the art in counterpoise theory, *Chemical Reviews* **94**, 1873 (1994).
- [44] D. Sheppard, R. Terrell, and G. Henkelman, Optimization methods for finding minimum energy paths, *The Journal of Chemical Physics* **128**, 134106 (2008).
- [45] S. R. Barman and D. D. Sarma, Electronic structure of  $\text{TiO}_x$  ( $0.8 < x < 1.3$ ) with disordered and ordered vacancies, *Phys. Rev. B* **49**, 16141 (1994).
- [46] There is also a difference in the supercell size, however we don't think it plays an important role, in view of quite localized character of hydrogen vibrations.
- [47] R. Kirchheim and A. Pundt, 25 – hydrogen in metals, in *Physical Metallurgy (Fifth Edition)*, edited by D. E. Laughlin and K. Hono (Elsevier, Oxford, 2014) fifth edition ed., pp. 2597–2705.
- [48] G. Mills and H. Jónsson, Quantum and thermal effects in  $\text{H}_2$  dissociative adsorption: Evaluation of free energy barriers in multidimensional quantum systems, *Phys. Rev. Lett.* **72**, 1124 (1994).
- [49] R. Gomer, Diffusion of adsorbates on metal surfaces, *Reports on Progress in Physics* **53**, 917 (1990).
- [50] V. P. Zhdanov, Arrhenius parameters for rate processes on solid surfaces, *Surface Science Reports* **12**, 185 (1991).
- [51] H. K. Birnbaum and C. P. Flynn, Hydrogen tunneling states in niobium, *Phys. Rev. Lett.* **37**, 25 (1976).
- [52] K. W. Kehr, Theory of the diffusion of hydrogen in metals, in *Hydrogen in Metals I: Basic Properties*, edited by G. Alefeld and J. Völkl (Springer Berlin Heidelberg, Berlin, Heidelberg, 1978) pp. 197–226.
- [53] M. Pozzo and D. Alfè, Hydrogen dissociation and diffusion on transition metal (=Ti, Zr, V, Fe, Ru, Co, Rh, Ni, Pd, Cu, Ag)-doped Mg(0001) surfaces, *International Journal of Hydrogen Energy* **34**, 1922 (2009).
- [54] A. Gringoz, N. Glandut, and S. Valette, Electrochemical hydrogen storage in  $\text{TiC}_{0.6}$ , not in  $\text{TiC}_{0.9}$ , *Electrochemistry Communications* **11**, 2044 (2009).
- [55] J. Nguyen, N. Glandut, C. Jaoul, and P. Lefort, Hydrogen insertion in substoichiometric titanium carbide, *International Journal of Hydrogen Energy* **40**, 8562 (2015).
- [56] J. M. Schoen and S. P. Denker, Band structure, physical properties, and stability of  $\text{TiO}$  by the augmented-plane-wave virtual-crystal approximation, *Phys. Rev.* **184**, 864 (1969).